Magnetic Susceptibility Tensor and Heme Contact Shifts Determinations in the *Rhodobacter capsulatus* Ferricytochrome *c*′: NMR and Magnetic Susceptibility Studies

Pascale Tsan,[†,||] Michael Caffrey,[†,⊥] Max Lawson Daku,[‡,#] Michael Cusanovich,[§] Dominique Marion,[†] and Pierre Gans*[,†]

Contribution from the Institut de Biologie Structurale "Jean-Pierre Ebel" (CEA-CNRS), 41 Avenue Jules Horowitz, 38027 Grenoble Cedex, France, DRFMC-SCIB-SCPM, 85X, CEN-Grenoble, 38041 Grenoble Cedex, France, and Department of Biochemistry, University of Arizona, Tucson, Arizona 85721

Received April 3, 2000. Revised Manuscript Received December 26, 2000

Abstract: The ^{1}H and ^{15}N resonances of the carbon monoxide complex of ferrocytochrome *c*′ of *Rhodobacter capsulatus*, a ferrous diamagnetic heme protein, have been extensively assigned by TOCSY−HSQC, NOESY−HSQC, and HSQC−NOESY−HSQC 3D heteronuclear experiments performed on a 7 mM sample labeled with ^{15}N. Based on short-range and medium-range NOEs and H^N exchange rates, the secondary structure consists of four helices: helix 1 (3−29), helix 2 (33−48), helix 3 (78−101), and helix 4 (103−125). The ^{15}N, $^{1}H^N$, and $^{1}H^{\alpha}$ chemical shifts of the CO complex form are compared to those of the previously assigned oxidized (or ferric) state. From the chemical shift differences between these redox states, the orientation and the anisotropy of the paramagnetic susceptibility tensor have been determined using the crystallographic coordinates of the ferric state. The χ-tensor is axial, and the orientation of the *z*-axis is approximately perpendicular to the heme plane. The paramagnetic chemical shifts of the protons of the heme ligand have been determined and decomposed into the Fermi shift and dipolar shift contributions. Magnetic susceptibility studies in frozen solutions have been performed. Fits of the susceptibility data using the model of Maltempo (Maltempo, M. M. *J. Chem. Phys.* **1974**, *61*, 2540−2547) are consistent with a rather low contribution of the $S = {}^{3}/_{2}$ spin state over the range of temperatures and confirm the value of the axial anisotropy. Values in the range 10.4−12.5 cm^{-1} have been inferred for the axial zero-field splitting parameter (*D*). Analysis of the contact shift and the susceptibility data suggests that cytochrome *c*′ of *Rb. capsulatus* exhibits a predominant high-spin character of the iron in the oxidized state at room temperature.

Introduction

The cytochromes *c*′ (Cytc′)[1] are class II cytochromes *c*, characterized by heme attachment to the C-terminal region of the protein, histidine as an axial ligand, the absence of a second axial ligand, and a low redox potential varying from −10 to +150 mV.[2,3] Cytc′ generally are dimers composed of two identical 13 kDa subunits, each of which consists of a four-helix bundle structural motif,[4−6] although monomeric species have been characterized in *Rhodopseudomonas palustris*[7] and in *Rhodobacter capsulatus* strains.[8] Roles in the metabolic pathway of photosynthesis,[4] nitrogen assimilation,[3] or NO detoxification[9] have been suggested, but their physiological role remains unclear. The major physiological state of the Cytc′ is

* To whom correspondence should be addressed. E-mail: pierre.gans@ibs.fr. Telephone: (33) 476885798. Fax: (33) 476885494.

† Institut de Biologie Structurale "Jean-Pierre Ebel".

‡ CEN-Grenoble.

§ University of Arizona.

|| Present address: Laboratoire de RMN Biomoléculaire, Université Claude Bernard-Lyon 1, 69622 Villeurbanne Cedex, France.

⊥ Present address: Department of Biochemistry and Molecular Biology, University of Illinois, Chicago, IL 60612.

Present address: Département de Chimie Physique, Universite de Genève-Sciences II, CH-1211 Genève 4, Switzerland.

(1) Abbreviations: Cytc′, cytochrome *c*′; HMQC, heteronuclear multiple quantum coherence spectroscopy; HSQC, heteronuclear single quantum coherence spectroscopy; NMR, nuclear magnetic resonance; NOE, nuclear Overhauser effect; NOESY, nuclear Overhauser enhancement spectroscopy; TOCSY, total correlated spectroscopy; TPPI, time proportional phase incrementation; WATERGATE, water suppression by gradient-tailored excitation; EPR, electron paramagnetic resonance; MCD, magnetic circular dichroism; EXAFS, extended X-ray absorption fine structure; ZFS, zero-field splitting.

(2) Bartsch, R. G. In *The Photosynthetic Bacteria*; Clayton, R. K., Sistrom, W. R., Eds.; Plenum: New York, 1978; pp 249−280. Meyer, T. E.; Kamen, M. D. *Adv. Protein Chem.* **1982**, *35*, 105−212. Pettigrew, G. W.; Moore, G. R. In *Cytochromes c: Biological aspects*; Springer-Verlag: Berlin, 1987.

(3) Yamanaka, T. In *The Biochemistry of Bacterial Cytochromes*; Japan Scientific Societies Press: Tokyo, 1992; pp 89−168.

(4) Moore, G. R.; Pettigrew, G. W. In *Cytochromes c: Evolutionary, Structural and Physicochemical aspects*; Springer-Verlag: Berlin, 1990.

(5) Weber, P. C.; Howard, A. J.; Xuong, N. H.; Salemme, F. R. *J. Mol. Biol.* **1981**, *153*, 399−424. Finzel, B. C.; Weber, P. C.; Hardman, K. D.; Salemme, F. R. *J. Mol. Biol.* **1985**, *186*, 627−643. Yasui, M.; Harada, S.; Kai, Y.; Kasai, N.; Kusunoki, M.; Matsuura, N. *J. Biochem. (Tokyo)* **1992**, *111*, 317−324. Ren, Z.; Meyer, T. E.; McRee, D. E. *J. Mol. Biol.* **1993**, *234*, 433−445. Dobbs, A. J.; Anderson, B. F.; Faber, H. R.; Baker, E. N. *Acta Crystallogr.* **1996**, *D52*, 356−368.

(6) Tahirov, T. H.; Misaki, S.; Meyer, T. E.; Cusanovich, M. A.; Higuchi, Y.; Yasuoka, N. *Nature, Struct. Biol.* **1996**, *3*, 459−464. Tahirov, T. H.; Misaki, S.; Meyer, T. E.; Cusanovich, M. A.; Higuchi, Y.; Yasuoka, N. *J. Mol. Biol.* **1996**, *259*, 467−479.

(7) Cusanovich, M. A. *Biochim. Biophys. Acta* **1971**, *236*, 238−241. Shibata, N.; Iba, S.; Misaki, S.; Meyer, T. E.; Bartsch, R. G.; Cusanovich, M. A.; Morimoto, Y.; Higuchi, Y.; Yasuoka, N. *J. Mol. Biol.* **1998**, *284*, 751−760.

(8) Tahirov, T. H.; Misaki, S.; Meyer, T. E.; Cusanovich, M. A.; Higuchi, Y.; Yasuoka, N. *Acta Crystallogr.* **1997**, *D53*, 658−664. Demene, H.; Tsan, P.; Gans, P.; Marion, D. *J. Phys. Chem. B* **2000**, *104*, 2559−2569.

(9) Cross, R.; Aish, J.; Paston, S. J.; Poole, R. K.; Moir, J. W. B. *J. Bacteriol.* **2000**, *182*, 1442−1447.

10.1021/ja0011663 CCC: $20.00
Published on Web 02/15/2001

probably the reduced state, as the typical EPR signal of ferriCytc′ is not detected in vivo.[10] On another hand, although purified ferroCytc′ binds CO, intact cells do not bind the CO expected from their Cytc′ content.[11]

Cytochromes *c′* have been studied widely in their oxidized state by numerous techniques: NMR,[12] EPR,[13−15] Mössbauer,[16] MCD,[17] resonance Raman,[18] and EXAFS spectroscopy.[19] Indeed, at low temperature, the Cytc′ of *Chromatium vinosum* presents an unusually low magnetic moment ($\mu_{eff} = 3.6\ \mu_B$) and EPR maximal absorption ($g = 4.8$) in the oxidized (or ferric) state at neutral and acidic pH.[14] Maltempo has proposed the existence of a quantum mechanical mixed state of high and intermediate-spin ($S = {}^5/_2$ and ${}^3/_2$) states in order to explain these magnetic properties.[14,20] However, further studies have shown that this feature is not conserved among the Cytc′, which can be divided into two groups on the basis of their EPR properties. A first group presents a large $S = {}^3/_2$ state contribution: *Rb. capsulatus*,[10d,15b] *Rps. palustris*[15b] or *Achromobacter xylosydans N.C.I.B. 11015* strain[15a] (former *Alcaligenes* sp. *N.C.I.B.*) (40% of $S = {}^3/_2$ state contribution), and *C. vinosum*[14,15b] (50− 70%). In the second group, only the $S = {}^5/_2$ state is observed: *Rhodospirullum molischianum*,[15b] *Rhodospirullum rubrum*,[15b] *Methylococcus capsulatus* Bath,[15c] or several strains of *A. xylosydans*.[14] Moreover, ambiguities on the exact contribution of the intermediate-spin state, even in the same species, remain to be elucidated. EXAFS or UV−visible spectroscopy suggests a significant contribution of the intermediate-spin state for *Rsp. molischianum*,[19] *Rsp. rubrum*,[19] *Rb. capsulatus*,[10d] or *A. xylosydans*.[15a] In contrast, MCD[17] and NMR[12d] studies of several cytochromes c′ (*Rsp. molischianum*, *Rsp. rubrum*, *Rps. palustris*, and *C. vinosum)* suggest that these species (except for *C. vinosum*) present an essentially high-spin character at room temperature. It is noteworthy that cytochromes *c′* exhibit similar pyrrolic methyl chemical shifts regardless of the proportion of the admixed spin states. Indeed, pyrrolic methyl protons exhibit large downfield chemical shifts, generally indicative of large *σ*-delocalization associated with the electronic half-occupancy of the highest d-iron orbital.[21] No characterization of the Fermi contact shifts in these compounds has, however, been performed, and this interpretation remains debatable. This led us to investigate the Fermi contact shifts of the iron ligands in the oxidized state of the ferriCytc′ of *Rb. capsulatus*, described by EPR[10d,15b] as a (40% ${}^3/_2$, 60% ${}^5/_2$) quantum-admixed spin state.

In paramagnetic proteins such as ferricytochromes *c′*, the observed chemical shift is described by

$$\delta_{obs} = \delta_{dm} + \delta_{pm} \quad (1)$$

where δ_{obs}, δ_{dm}, and δ_{pm} are the observed, diamagnetic, and paramagnetic (or hyperfine) shifts, respectively. The paramagnetic shift arises from two contributions: the Fermi contact shift (δ_{con}) due to spin density delocalization along the chemical bonds and the dipolar shift (δ_{dip}) linked to the dipolar field induced by the electronic spin.[22] For nuclei not coupled through scalar coupling to the paramagnetic center, δ_{pm} reduces to the dipolar (or pseudocontact) effect and is described by the following general equation:[22]

$$\delta_{pm} = (1/12\pi N_a)[(\chi_{zz} - 1/2(\chi_{xx} + \chi_{yy}))(3\cos^2\Theta - 1)/r^3 + 3/2(\chi_{xx} - \chi_{yy})(\sin^2\Theta\cos 2\phi)/r^3] \quad (2)$$

where N_a is the Avogadro's number, χ_{xx}, χ_{yy}, and χ_{zz} are the principal components of the molar magnetic susceptibility tensor χ, and r, Θ, and ϕ are the polar coordinates of the nucleus in the reference frame defined by the principal axes of the χ-tensor with the origin at the electronic density center.

Thus, provided that the protein structure, from which the geometric factors r, Θ, and ϕ can be inferred, has been independently determined either by X-ray crystallography or by NMR, the measurement of the dipolar shift allows one to characterize the orientation and the magnitude of the magnetic susceptibility tensor. In high-spin hemoproteins, this shift generally arises from the existence of a significant zero-field splitting (ZFS), and the susceptibility values in eq 2 are given by

$$\Delta\chi_{ax} = \chi_{zz} - \frac{1}{2}(\chi_{xx} + \chi_{yy}) = -\left[\frac{S(S+1)(2S-1)(2S+3)\,g^2\beta^2}{30k^2T^2}\right]D \quad (3)$$

$$\Delta\chi_{rh} = (\chi_{xx} - \chi_{yy}) = -\left[\frac{S(S+1)(2S-1)(2S+3)g^2\beta^2}{30k^2T^2}\right]2E \quad (4)$$

(10) Dutton, P. L.; Leigh, J. S. *Biochim. Biophys. Acta* **1973**, *314*, 178−190. (b) Prince, R. C.; Leigh, J. S.; Dutton, P. L. *Biochem. Soc. Trans.* **1974**, *2*, 950−953. (c) Corker, G. A.; Sharpe, S. A. *Photochem. Photobiol.* **1975**, *21*, 49−61. (d) Monkara, F.; Bingham, S. J.; Kadir, F. H. A.; McEwan, A. G.; Thomson, A. J.; Thurgood, A. G. P.; Moore, G. R. *Biochim. Biophys. Acta* **1992**, *1100*, 184−188.

(11) Cusanovich, M. A.; Bartsch, R. G.; Kamen, M. D. *Biochim. Biophys. Acta* **1968**, *153*, 397−417.

(12) Emptage, M. H.; Xavier, A. V.; Wood, J. M.; Alsaadi, B. M.; Moore, G. R.; Pitt, R. C.; Williams, R. J. P.; Ambler, R. P.; Bartsch, R. G. *Biochemistry* **1981**, *20*, 58−64. (b) Jackson, J. T.; La Mar, G. N.; Bartsch, R. G. *J. Biol. Chem.* **1983**, *258*, 1799−1805. (c) Akutsu, H.; Kyogoku, Y.; Horio, T. *Biochemistry* **1983**, *22*, 2055−2063. (d) La Mar, G. N.; Jackson, J. T.; Dugad, L. B.; Cusanovich, M. A.; Bartsch, R. G. *J. Biol. Chem.* **1990**, *265*, 16173−16180. (e) Banci, L.; Bertini, I.; Turano, P.; Vicens Olivier, M. *Eur. J. Biochem.* **1992**, *204*, 107−112. (f) Bertini, I.; Gori, G.; Luchinat, C.; Vila, A. *Biochemistry* **1993**, *32*, 776−783. (g) Caffrey, M.; Simorre, J.-P.; Brutscher, B.; Cusanovich, M. A.; Marion, D. *Biochemistry* **1995**, *34*, 5904−5912. (h) Caffrey, M.; Simorre, J.-P.; Cusanovich, M. A.; Marion, D. *FEBS Lett.* **1995**, *368*, 519−522. (i) Clark, K.; Dugad, L. B.; Bartsch, R. G.; Cusanovich, M. A.; La Mar, G. N. *J. Am. Chem. Soc.* **1996**, *118*, 4654−4664.

(13) Ehrenberg, A.; Kamen, M. D. *Biochim. Biophys. Acta* **1965**, *102*, 333−340.

(14) Maltempo, M. M. *J. Chem. Phys.* **1974**, *61*, 2540−2547.

(15) Yoshimura, T.; Suzuki, S.; Nakahara, A.; Iwasaki, H.; Masuko, M.; Matsubara, T. *Biochim Biophys Acta* **1985**, *831*, 267−274. (b) Fujii, S.; Yoshimura, T.; Kamada, H.; Yamaguchi, K.; Suzuki, S.; Shidara, S.; Takakuwa, S. *Biochim. Biophys. Acta* **1995**, *1251*, 161−169. (c) Zahn, J. A.; Arciero, D. M.; Hooper, A. B.; Dispirito, A. A. *Eur. J. Biochem.* **1996**, *240*, 684−691.

(16) Moss, T. H.; Bearden, A. J.; Bartsch, R. G.; Cusanovich, M. A. *Biochemistry* **1968**, *7*, 1583−1590. Emptage, M. H.; Zimmermann, R.; Que, L., Jr.; Münck, E.; Hamilton, W. D.; Orme-Johnson, W. H. *Biochim. Biophys. Acta* **1977**, *495*, 12−23. Maltempo, M. M.; Moss, T. H.; Spartalian, K. *J. Chem. Phys.* **1980**, *73*, 2100−2106.

(17) Rawlings, J.; Stephens, P. J.; Nafie, L. A.; Kamen, M. D. *Biochemistry* **1977**, *16*, 1725−1729.

(18) Strekas, T. C.; Spiro, T. G. *Biochim. Biophys. Acta* **1974**, *351*, 237−245. Kitagawa, T.; Ozaki, Y.; Kyogoku, Y.; Horio, T. *Biochim. Biophys. Acta* **1977**, *495*, 1−11. Hobbs, J. D.; Larsen, R. W.; Meyer, T. E.; Hazzard, J. H.; Cusanovich, M. A.; Ondrias, M. R. *Biochemistry* **1990**, *29*, 4166−4174. Othman, S.; Richaud, P.; Verméglio, A.; Desbois, A. *Biochemistry* **1996**, *35*, 9224−9234.

(19) Korszun, Z. R.; Bunker, G.; Khalid, S.; Scheidt, W. R.; Cusanovich, M. A.; Meyer, T. E. *Biochemistry* **1989**, *28*, 1513−1517.

(20) Maltempo, M. M.; Moss, T. H. *Q. Rev. Biophys.* **1976**, *9*, 181−215.

(21) Walker, F. A.; Simonis, U. In *Biological Resonance NMR*; Berliner, L. J., Reuben, J., Eds.; Plenum Press: New York, 1993; Vol. 12, pp 133−274.

where *D* and *E* are the axial and rhombic zero-field splitting parameters.[22,23]

To our knowledge, very few NMR studies of high-spin ferric heme proteins have used chemical shift differences between redox states to derive *D* and probe for structural differences between redox states.[24] As the reduced state is also paramagnetic, the lack of a diamagnetic reference prevents the use of eq 1 for this purpose. As yet, such a study has not been performed for a ferriCytc′. However, the observed chemical shifts of protons located in the heme cavity are in agreement, for the monomeric Cytc′ of *Rps. palustris*, with the shifts predicted using a *D* value typical of high-spin iron proteins and a model built from the structure of the *Rsp. molischianum* Cytc′.[12i]

In the present article, we present the characterization of the magnetic properties of the iron in the *Rb. capsulatus* ferriCytc′. For this purpose, we have first assigned the carbon monoxide ferroCytc′ diamagnetic complex by a combination of 3D heteronuclear and 2D homonuclear experiments. We have determined the orientation of the magnetic susceptibility tensor and the magnetic anisotropy in the oxidized state from $^1H^N$ and $^1H^\alpha$ chemical shift differences between the previously assigned oxidized form[12g] and the diamagnetic complex. The respective contributions of the Fermi contact shift and the dipolar shift in the heme protons chemical shifts have been separated, and the Fermi contact shift variations have been analyzed as functions of temperature and pH. Magnetic susceptibility measurements performed in the range 6−250 K have been interpreted with the quantum-admixed spin state model of Maltempo.[14]

Materials and Methods

Protein Preparation. Preparation of unlabeled and ^{15}N-labeled *Rb. capsulatus* Cytc′ has been previously described.[12g] For the assignment experiments, the ^{15}N-labeled sample was concentrated at 4 °C to approximately 7 mM (heme concentration) in buffer containing 100 mM PO_4 (pH 6.0). Oxygen was removed by blowing argon gas over the solution surface for approximately 15 min. The sample was reduced by the addition of approximately 10 mg of sodium dithionite (Janssen Chimica), the sample was flushed with carbon monoxide, and the tube was closed with a septum cap. For the pH experiments, the unlabeled ferriCytc′ sample was concentrated at 0.5−1 mM in pure ^2H_2O. The solution pH was adjusted by ^{2}HCl or NaO^{2}H. The pH values were measured on a PHN 81 Tacussel pH meter using an MI-412 microelectrode (Microelectrodes, Inc). The reported pH values were not corrected for the isotope effect. For the NMR experiments performed as a function of the temperature, unlabeled ferriCytc′ sample was concentrated in a buffer containing 100 mM PO_4 at pH 6.0. For the EPR experiment, a frozen solution at 0.5 mM unlabeled ferriCytc′ in buffer containing 100 mM phosphate buffer at pH 6.0 was used. For the magnetic susceptibility measurements, the sample of ferriCytc′ was dialyzed against a 100 mM phosphate buffer at pH 6.0, lyophilized overnight, and redissolved in pure ^2H_2O (Eurisotop, 99.9%).

NMR Experiments. NMR experiments were performed on Bruker AMX400 and AMX600 spectrometers equipped with ^{1}H and ^{15}N double-resonance probes operating at a temperature of 300 K. TOCSY[25] and NOESY[26] spectra were recorded in the phase-sensitive mode using the hypercomplex method.[27] ^{15}N was decoupled using a GARP scheme with 1.9 kHz field strength. Water resonance was attenuated by means of a coherent low-power presaturation during the relaxation delay further combined with a "jump and return" read pulse.[28] The WALTZ-17 mixing scheme used in TOCSY experiments was optimized for balancing longitudinal and rotating frame cross-relaxation according to the technique known as clean TOCSY.[29] TOCSY spectra were recorded with an isotropic mixing time of 60 ms including the delays of the clean TOCSY pulse scheme; the field strength of the spin lock was 10 kHz. The NOESY spectra were recorded with mixing times of 80 and 120 ms. Two-dimensional spectra were collected as 512 (t_1) and 1024 (t_2) complex points with 32 scans per t_1 increment. Chemical shifts were referenced relative to the water resonance fixed at 4.75 ppm at 300 K. 2D HSQC experiments were recorded with 11 and 30 ppm spectral width for the ^{1}H and ^{15}N dimensions and centered at 4.75 and 119.3 ppm, respectively. Spectra were acquired with 150 complex points in t_1 and 16 scans per t_1 increment for a total experimental time of approximately 1 h. The 3D TOCSY−HSQC, NOESY−HSQC, and HSQC−NOESY−HSQC experiments were similar to the TOCSY−HMQC,[30] NOESY−HMQC,[31] and HMQC−NOESY−HMQC[32] experiments previously described except for the following modifications: the HSQC sequence[33] was used as opposed to the HMQC sequence to increase the resolution of the ^{15}N dimension, and pulsed field gradients[34] were added to suppress undesired coherence transfer pathways. Solvent suppression was accomplished by using the WATERGATE sequence[35] and selective water flip-back pulses. The field strength for WALTZ-16 decoupling[36] of ^{15}N was 1.9 kHz. Quadrature detection in the indirectly detected dimensions was obtained by the TPPI−States method.[37] For the TOCSY−HSQC and NOESY−HSQC experiments, the spectral widths for ^{1}H, ^{15}N, and ^{1}H were 11, 30, and 11 ppm, respectively; carrier positions for ^{1}H, ^{15}N, and ^{1}H were 4.75, 119.3, and 4.75 ppm, respectively. Spectra were acquired with 180 complex points in t_1, 120 complex points in t_2, and 8 scans per t_1/t_2 increment, resulting in a total experimental time of approximately 60 h. For the TOCSY−HSQC experiment, the isotropic mixing time was 60 ms (including delays), and the field strength of the ^{1}H WALTZ-16 spin lock was 10 kHz. For the HSQC−NOESY−HSQC experiment, the spectral widths for ^{15}N, ^{15}N, and ^{1}H were 30, 30, and 11 ppm, respectively; carrier positions for ^{15}N, ^{15}N, and ^{1}H were 119.3, 119.3, and 4.75 ppm, respectively. Spectra were acquired with 120 complex points in t_1, 120 complex points in t_2, and 16 scans per t_1/t_2 increment, resulting in a total experimental time of approximately 85 h. For the NOESY−HSQC and HSQC−NOESY−HSQC experiments, the mixing time was 120 ms.

All data were processed using the FELIX program version 97 (Molecular Simulation Inc.). The indirect dimensions of 2D data sets were multiplied by a skewed sine bell function and zero-filled to result in 1024×256 matrixes for HSQC spectra. 3D data sets were multiplied by a Gaussian function in the acquisition dimension and a skewed sine bell function in the indirect dimension and zero-filled prior to Fourier transform. Final 3D matrixes were 512×128×256 real points for the TOCSY−HSQC, NOESY−HSQC, and HSQC−NOESY−HSQC. For convenient analysis of 3D data sets, 2D strips were generated as previously described.[38]

(22) Jesson, J. P. In *NMR of Paramagnetic Molecules. Principles and Applications*; La Mar, G. N., Horrocks, W. DeW., Jr., Holm, R. H., Eds.; Academic Press: New York, 1973; pp 2−52.
(23) Kurland, R. J.; McGarvey, B. R. *J. Magn. Reson.* **1970**, *2*, 286−301.
(24) Rajarathnam, K.; La Mar, G. N.; Chiu, M. L.; Sligar, S. G.; Singh, J. P.; Smith, K. M. *J. Am. Chem. Soc.* **1991**, *113*, 7886−7892. Kao, Y.-H.; Lecomte, J. T. J. *J. Am. Chem. Soc.* **1993**, *115*, 9754−9762.
(25) Braunschweiler, L.; Ernst, R. R. *J. Magn. Reson.* **1983**, *53*, 521−528. Davis, D. G.; Bax, A. *J. Am. Chem. Soc.* **1985**, *107*, 2820−2821.
(26) Jeener, J.; Meier, B. H.; Bachmann, P.; Ernst, R. R. *J. Chem. Phys.* **1979**, *71*, 4546−4553. Macura, S.; Hyang, Y.; Suter, D.; Ernst, R. R. *J. Magn. Reson.* **1981**, *43*, 259−281.
(27) States, D. J.; Haberkorn, R. A.; Ruben, D. J. *J. Magn. Reson.* **1982**, *48*, 286−292.
(28) Plateau, P.; Guéron, M. *J. Am. Chem. Soc.* **1982**, *104*, 7310−7311.
(29) Griesinger, C.; Otting, G.; Wüthrich, K.; Ernst, R. R. *J. Am. Chem. Soc.* **1988**, *110*, 7870−7872.
(30) Marion, D.; Driscoll, P. C.; Kay, L. E.; Wingfield, P. T.; Bax, A.; Gronenborn, A. M.; Clore, G. M. *Biochemistry* **1989**, *28*, 6150−6156.
(31) Kay, L. E.; Marion, D.; Bax, A. *J. Magn. Reson.* **1989**, *84*, 72−84.
(32) Ikura, M.; Bax, A.; Clore, G. M.; Gronenborn, A. M. *J. Am. Chem. Soc.* **1990**, *112*, 9020−9026.
(33) Bodenhausen, G.; Ruben, D. J. *Chem. Phys. Lett.* **1980**, *69*, 185−189.
(34) Bax, A.; Pochapsky, S. S. *J. Magn. Reson.* **1992**, *99*, 638−643.
(35) Sklenàr, V.; Piotto, M.; Leppik, R.; Saudek V. *J. Magn. Reson.* **1993**, *102*, 241−245.
(36) Shaka, A. J.; Keeler, J.; Frenkiel, T.; Freeman, R. *J. Magn. Reson.* **1983**, *52*, 335−338.
(37) Marion, D.; Ikura, M.; Tschudin, R.; Bax, A. *J. Magn. Reson.* **1989**, *85*, 393−399.

Computer Modeling. The geometric factors were calculated using the crystallographic structure of *Rb. capsulatus* ferriCytc′ at 1.72 Å resolution.[6] For this analysis, the program Insight II (Molecular Simulations, Inc.) was used to add proton coordinates. The reference frame was defined as having the origin at the iron, the *Z*-axis perpendicular to the pyrrole nitrogen plane, the *X*-axis nearly along the N(III)−N(I) direction, and the *Y*-axis along the N(IV)−N(II) direction. All the calculations were performed for both crystallographic subunits of the dimer in order to account for possible differences in the atom positions.

The magnetic susceptibility tensor (χ_{xx}, χ_{yy}, χ_{zz}) is oriented by means of three Euler angles α, β, and γ relative to the molecular reference axes described above. The two anisotropic components of the magnetic tensor were obtained from eq 2 as previously described.[39] The optimization of the Euler angles α, β, and γ and the two components $\Delta\chi_{ax}$ and $\Delta\chi_{rh}$ was achieved by means of a simulated annealing algorithm developed in our laboratory.[40] In the case of an axially symmetric χ tensor, the direction of the symmetry axis is defined only by β (tilt angle relative to *Z*) and α (direction of its projection onto the *XY* plane); thus, only three parameters were optimized in the calculation: $\Delta\chi_{ax}$, α, and β. As the axes *x*, *y*, and *z* are arbitrary, this gives up to six pairs of values of $\Delta\chi_{ax}$ and $\Delta\chi_{rh}$ related to one another by circular permutation of the *x*, *y*, and *z* axes. The axes have been arbitrarily chosen with the largest component along *z* and the smallest along *x* (i.e., $|\chi_{zz}| > |\chi_{yy}| > |\chi_{xx}|$) as previously described.[39] Structural changes were detected as for the reduced form[39] using the criterion defined by Feng et al.[41]

Magnetic Susceptibility Measurements. Data were collected on a 100-μL sample of ferriCytc′ at 3 mM heme concentration in ^2H_2O with an SHE model 905 SQUID susceptometer. Before the measurements, the quartz sample holder was first left overnight in a HF solution to eliminate ferromagnetic contaminants, washed in twice-distilled water, sonicated, and rinsed with twice-distilled water. Measurements were made between 6 K and room temperature for two magnetic fields, 0.5 and 1 T. The data were first corrected for the empty holder contribution, recorded under the same conditions. The diamagnetic contribution χ_{dia} from the protein and ^2H_2O was evaluated assuming that the magnetization follows a polynomial law at high temperatures:

$$M(H,1/T) = a_H + b_H T^{-1} + c_H T^{-2} \quad (5)$$

where a_H is an estimate of χ_{dia}. This value was then subtracted from the experimental data.[42] Values of a_H were found to be -6.322099×10^{-8} emu at 0.5 T and -6.601557×10^{-8} emu at 1 T. The holder contribution and the magnetic susceptibility data corrected from this contribution are given in the Supporting Information (Tables S1, S2, and S3).

Fits of the data were made using two different models. The first one assumes that the system is in a pure spin state and is described by the classical effective spin Hamiltonian:[43]

$$H = \beta S\mathbf{g}H + D[S_z^2 - 1/3\ S(S+1)] + E(S_x^2 - S_y^2) \quad (6)$$

where *D* and E are the ZFS axial and rhombic factors, respectively, and the **g**-tensor is taken as isotropic.

The second approach uses the model developed by Maltempo,[14] where the $^5/_2$ and $^3/_2$ states are separated in energy by the crystal field parameter Δ but are sufficiently close to be mixed together through spin−orbit interaction λ. No rhombicity is introduced in this approach.

Data were adjusted by minimization of the residual:

$$R = \sum_i \left((M_{obs}(T_i,H_i) - M_{calc}(T_i,H_i)) \frac{T_i}{H_i} \right)^2 \quad (7)$$

using the nearest-neighbor pivot method.[44] The calculated magnetization value $M(T_i,H_i)$ is given by the formula

$$M(T_i,H_i) = nN_a k_B T_i \int \sin\Theta\, d\Theta \int \frac{\partial\phi}{4\pi} \left[\frac{\partial(\ln Z(T_i,H,\Theta,\phi))}{\partial H} \right]_{H=H_i} \quad (8)$$

where N_a is Avogadro's number, and $Z(T_i,H,\Theta,\phi)$ is the system partition function for an orientation Θ,ϕ in the magnetic field system's frame of reference.[43]

Results

Assignment of the Carbon Monoxide Complex of Ferrocytochrome *c*′. (a) Spin System Identification. In the TOCSY−HSQC 3D experiment, intraresidue $^1H^N-^1H^\alpha$ correlations were observed for 118 of 126 amino acids (accounting for three prolines). Six supplementary correlations were detected in a 2D TOCSY. $^1H^N-^1H^\beta$ correlations were observed for 70 of 112 amino acids (accounting for three prolines and 14 glycines) in a 3D HSQC−TOCSY experiment and 80 amino acids in a 2D TOCSY experiment. Using the aliphatic region of the 2D TOCSY and the 2D NOESY, 110 $^1H^N-^1H^\beta$ correlations have been identified. In contrast, many of the long-chain amino acids were missing correlations for the $^1H^\gamma$, $^1H^\delta$, or $^1H^\epsilon$, due to slow overall tumbling of the protein.[45]

(b) Sequential Assignment and Secondary Structure. The ^1H and ^{15}N resonances of *Rb. capsulatus* ferroCytc′ CO complex were sequentially assigned by the NOESY−HSQC 3D experiment, in which $^1H^N-^{15}N$ pairs are correlated to intra- and interresidue $^1H^{30}$ and the HSQC−NOESY−HSQC 3D experiment, in which $^1H^N-^{15}N$ pairs are correlated to interresidue ^{15}N.[32] Examples of the NOESY−HSQC spectra used for the assignment of residues A103 to R126 are given in Figure 1. In this figure, each residue is represented by a small region of the 2D plane at a given ^{15}N frequency and centered at a given $^1H^N$ frequency. Short-range $d_{NN(i,i+1)}$, $d_{\alpha N(i,i+1)}$, and $d_{\beta N(i,i+1)}$ connectivities are shown by horizontal lines. Due to the high helical content of Cytc′ (about 70%), HSQC−NOESY−HSQC have been found to be particularly useful to resolve ambiguities arising from spectral overlap. An example of the HSQC−NOESY−HSQC spectra used for the assignment of residues 33−37 is given in Figure 2. A summary of the short-range and medium-range ($d_{\alpha N(i,i+3)}$ and $d_{NN(i,i+2)}$) connectivities that were observed in the 3D NOESY−HSQC or 2D NOESY experiments is given in Figure 3. In addition, the relative H^N exchange rates are presented. Together, the $d_{\alpha N(i,i+3)}$ connectivities and H^N exchange rates suggest four helical regions in *Rb. capsulatus* CO−Cytc′ for residues 3−29, 33−48, 78−101, and 103−125. In total, backbone ^1H and ^{15}N resonances have been assigned for 124 of the 126 non-proline residues present in *Rb. capsulatus* Cytc′. During the assignment, two mistakenly described residues in the primary sequence[12g] were detected at positions 45 and 90 (D45 and D90). The better resolved spectra in the diamagnetic form allowed us to identify them unambiguously as a lysine at position 45 and, by homology with the primary sequence of the M110 strain,[6] as a glutamate in position 90.

(38) Caffrey, M.; Brutscher, B.; Simorre, J.-P.; Fitch, J.; Cusanovich, M. A.; Marion, D. *Eur. J. Biochem.* **1994**, *221*, 63−75.
(39) Tsan, P.; Caffrey, M.; Lawson Daku, M.; Cusanovich, M. A.; Marion, D.; Gans, P. *J. Am. Chem. Soc.* **1999**, *121*, 1795−1805.
(40) Blackledge, M.; Cordier, F.; Dosset, P.; Marion, D. *J. Am. Chem. Soc.* **1998**, *120*, 4538−4539.
(41) Feng, Y. Q.; Roder, H.; Englander, S. W. *Biochemistry* **1990**, *29*, 3494−3504.
(42) Day, E. P.; Kent, T. A.; Lindhal, P. A.; Münck, E.; Orme-Johnson, W. H.; Roder, H.; Roy, A. *Biophys. J.* **1987**, *52*, 837−853.
(43) Kahn, O. *Molecular Magnetism*; VCH Publishers: New York, 1993.
(44) Serra, P.; Stanton, A. F.; Kais, S. *J. Chem. Phys.* **1997**, *106*, 7170−7177.
(45) Tsan, P.; Hus, J.-C.; Caffrey, M.; Marion, D.; Blackledge, M. *J. Am. Chem. Soc.* **2000**, *122*, 5603−5612.

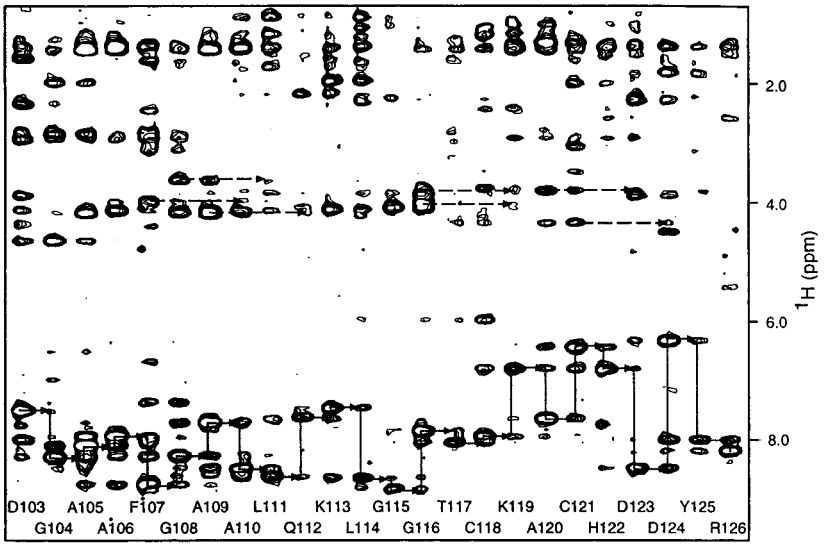

Figure 1. Strip representation of the NOESY−HSQC 3D experiment for the sequential assignment of the *Rb. capsulatus* ferrocytochrome *c′* CO complex residues D103−R126 (at pH 6, 27 °C). The mixing time was 120 ms. Each residue is presented as a 2D strip taken at the ^{15}N frequency and centered at the H^N frequency (Table S1, Supporting Information). Arrows are drawn in solid lines for (i, $i + 1$) NOE correlations and in dotted lines for (i, $i + 3$) correlations. The presence of consecutive d_{NN}'s is characteristic of a helical conformation between D103 and R126.

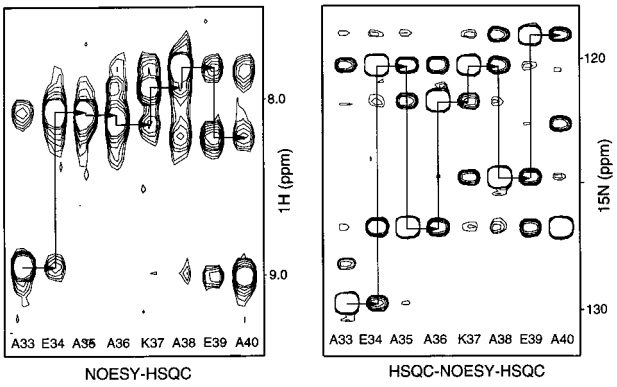

Figure 2. Strip representation of the NOESY−HSQC (left) and HSQC−NOESY−HSQC (right) 3D experiments for the sequential assignment of the *Rb. capsulatus* ferrocytochrome *c′* CO complex residues A33−A40 (at pH 6, 27 °C). The mixing time was 120 ms. Each residue is presented as a 2D strip taken at the ^{15}N frequency and centered at the H^N frequency (Table S1, Supporting Information). Arrows are drawn for interresidue NOEs. In the HSQC−NOESY−HSQC 2D representation, the resolution of consecutive d_{NN}'s using a second ^{15}N frequency allows the unambiguous assignment of the fragment A33−K37.

This determination has been also corroborated by mass spectrometry results (data not shown). The ^{1}H and ^{15}N chemical shifts of the monoxide complex of the ferroCytc′ are given in the Supporting Information (Table S4) and have been deposited in the BioMagResBank database (accession number 4761).

(c) Assignment of Side-Chain ^{15}NH. The side-chain ^{15}NH's of Q67, W75, N77, N100, and Q112 were identified by the TOCSY−HSQC 3D experiment and assigned by the NOESY−HSQC 3D experiment. The absence of a fifth NH_2 group is in agreement with the reassignment of residue 90 to Glu rather than Gln. Specifically, the side-chain H^N of W75 was assigned by a TOCSY correlation to the C2H, which exhibits NOEs to the previously assigned $^1H^\alpha$ and $^1H^\beta$ of W75. The side-chain ^{15}NH's of N77 and N100 were assigned by NOEs between the ^{15}NH and the previously assigned $^1H^\alpha$ and $^1H^\beta$. The side-chain ^{15}NH's of Q67 and Q112 were assigned by NOEs between the ^{15}NH and the previously assigned $^1H^\beta$ and $^1H^\gamma$. In contrast, the side-chain ^{15}NH's of R10, H89, H122, and R126 were not apparent in the TOCSY−HSQC or NOESY−HSQC 3D experiments.

(d) Assignment of the Iron Ligand Protons. The chemical shifts of the heme protons of the CO complex of Cytc′ are shown in Table 1. Assignments have been made following the procedure of Keller and Wüthrich.[46] Some propionate resonances have been identified from their correlations with the 15-H meso proton but could not be specifically assigned.

Magnetic Susceptibility Tensor Determination. Magnetic susceptibility tensor components as well as potential structural changes between redox states can be assessed from eq 2. It is, however, necessary to assume that the electronic density is localized at the iron center, a simplification that is only fully justified for nuclei located at more than 10 Å away from the metal center.[47] This criterion is satisfied by all of the protein backbone nuclei considered here. Dipolar shift in high-spin ferric hemoproteins is generally considered as resulting from a substantial ZFS axial parameter D only, since E is negligible and **g** isotropic. Dipolar shift is consequently given by eqs 2 and 3. So, we first assumed an axially symmetric χ tensor for the ferriCytc′ and kept only the first term of eq 2, thus deriving $\Delta\chi_{ax}$ and the orientation of the z axis tensor defined by the α and β angles. $^1H^N$ chemical shifts, which are sensitive to H-bonding,[48] were initially excluded from the calculation. ^{15}N chemical shifts were also excluded from the initial calculation, because they are sensitive to interactions between the ^{15}N atomic orbitals and those of neighboring atoms,[49] in addition to H-bonding. Glycine $^1H^\alpha$'s were excluded as they were not stereospecifically assigned. Therefore, in the initial stage, we used a set of 92 $^1H^\alpha$ resonances and the coordinates of subunit A of the X-ray structure. The fit resulted in $\Delta\chi_{ax} = -2.95 \times 10^{-8}$ m^3/mol, $\alpha = 176$, and $\beta = 2$ with a global residual $F/N = 5.49 \times 10^{-3}$ ppm^2 (Table 2). In Figure 4, the observed and calculated paramagnetic shifts are compared, which illustrates the very good agreement between these values. Using the B

(46) Keller, R. M.; Wüthrich, K. *Biochem. Biophys. Res. Commun.* **1978**, *83*, 1132−1139.
(47) Golding, R.; Pascual, R.; Stubbs, L. *Mol. Phys.* **1976**, *31*, 1933.
(48) Wagner, G.; Pardi, A.; Wuthrich, K. *J. Am. Chem. Soc.* **1993**, *105*, 5948−5949.
(49) Braun, D.; Wider, G.; Wuthrich, K. *J. Am. Chem. Soc.* **1994**, *116*, 8466−8469 and references therein.

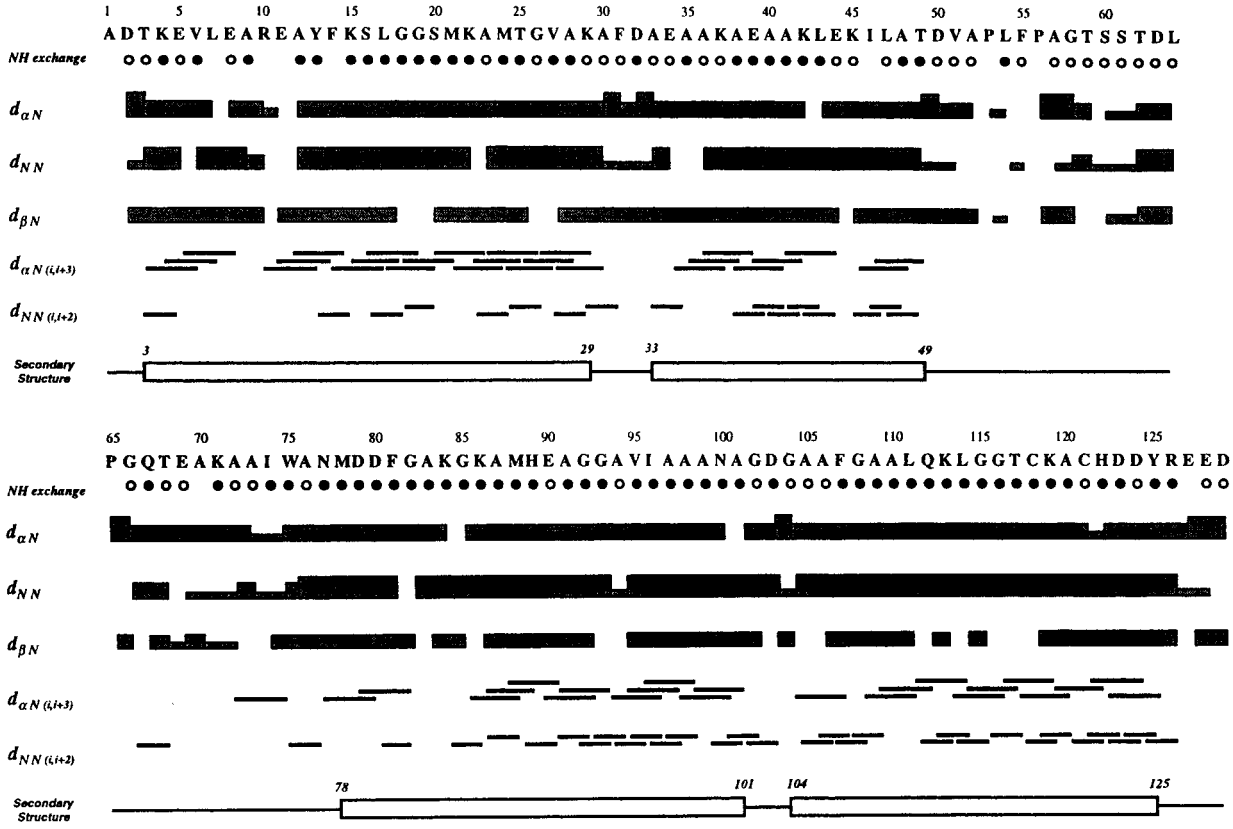

Figure 3. Schematic summary of the sequential connectivities for the assignment of the *Rb. capsulatus* ferrocytochrome *c*′ CO complex (at pH 6, 27 °C). Relative intensity is depicted by the box height. H^N's in slow exchange (detected after 2 h) are identified by filled circles, and H^N's in fast exchange (absent after 2 h) are identified by open circles. The helical regions identified by the $d_{\alpha N(i,i+3)}$ and slowly exchanging H^N's are shown by solid lines.

Table 1. Chemical Shifts of the Heme Protons in the Carbon Monoxide Complex of *Rhodobacter capsulatus* Ferrocytochrome *c*′

	chemical shift (ppm)[a]
5-meso	9.73
10-meso	9.92
15-meso	9.23
20-meso	9.99
Met-2	3.70
Met-7	3.79
Met-12	3.74
Met-18	3.60
Met-3	2.30
methine-3	6.00
Met-8	1.61
methine-8	5.89
13-Prop α	b
13-Prop β	b
17-Prop α	b
17-Prop β	b

[a] Chemical shifts are referenced to the H_2O resonance and defined with a ±0.02 ppm precision. [b] Resonances at 3.5, 2.95, 2.87, and 2.75 ppm have been identified as H-propionates but could not be specifically assigned.

Table 2. Calculated Angles and Components of the Magnetic Susceptibility Tensor for the Ferricytochrome *c*′ of *Rb. capsulatus*

atom set (subunit)	*a*, deg	*b*, deg	$\Delta\chi_{ax}$[a]	*F*/*N*[b]
Full Set				
92 H^α (A)	176	2	−2.95	5.49
92 H^α (B)	135	3	−2.90	4.24
103 H^N (A)	254	3	−2.93	3.77
103 H^N (B)	251	3	−2.94	3.18
103 ^{15}N (A)	165	3	−2.90	202
103 ^{15}N (B)	138	4	−2.91	202
92 H^α + 103 H^N (A)	231	2	−2.93	4.87
92 H^α + 103 H^N (B)	163	1	−2.94	3.90
Restricted Set				
64 H^α (A)	150	2	−3.02	3.89
65 H^α (B)	129	3	−2.99	3.33
95 H^N (A)	216	1	−2.94	3.18
96 H^N (B)	215	1	−2.94	2.89
67 H^α + 94 H^N (A)[c]	222 (4)	2 (1.3)	−2.94 (0.06)	4.30
67 H^α + 94 H^N (B)	164	1	−2.93	3.30

[a] In 10^{-8} m^3/mol. [b] In 10^{-3} ppm^2 [c] The numbers in parentheses correspond to the uncertainties calculated using Monte Carlo simulations.[51]

subunit coordinates led to a slightly lower residual *F*/*N* and similar $\Delta\chi_{ax}$ and β values. The large difference (39) found for α is actually meaningless here since the tilt angle β is almost zero. The $^1H^N$ and ^{15}N dipolar shifts calculated from the fit of the $^1H^\alpha$'s were plotted as a function of the experimental values (Figure 5). As illustrated by this figure, the agreement between predicted and observed shifts was very good for amide protons but poorer for nitrogens. Similarly to $^1H^\alpha$ shifts, fitting calculations have been performed with the sets of $^1H^N$ and ^{15}N shifts, as well as the combined set of $^1H^N$ and $^1H^\alpha$ shifts. The results obtained for each subunit are reported in Table 2. During this stage, we observed very large $^1H^\alpha$, $^1H^N$, or ^{15}N $\Delta\delta_{pm}$ for reported residues 69−74. Reexamination of the HSQC−NOESY led us to reassign these residues in the oxidized form, and the results are reported in Table S5.

In a second stage, the nuclei that exhibited significant discrepancies $|\Delta\Delta\delta|$ with the shifts calculated from the fitted parameters (see Material and Methods) (i.e., 28 $^1H^\alpha$, 8 $^1H^N$, and 20 ^{15}N of subunit A and 27 $^1H^\alpha$, 8 $^1H^N$, and 19 ^{15}N of subunit B)[50] were discarded from the calculation. We obtained slightly lower residuals but identical parameters. In contrast, using the

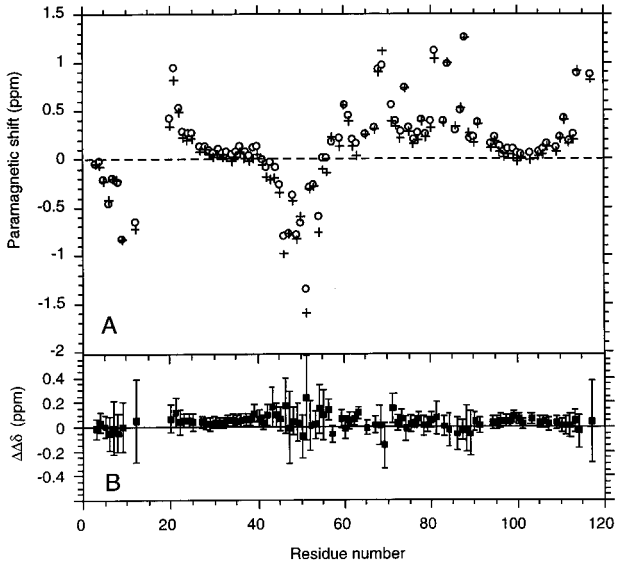

Figure 4. Comparison of the observed and calculated H^{α} paramagnetic chemical shifts for the ferricytochrome *c′* of *Rb capsulatus.* (A) Open circles, calculated paramagnetic chemical shifts; crosses, observed paramagnetic chemical shifts. Gly H^{α}'s were discarded for lack of stereospecific assignments. The H^{α} chemical shifts of residues 69−74 correspond to the reassigned values (see text). Values used for the calculation are $\alpha = 176°$, $\beta = 2°$, and $\Delta\chi_{ax} = -2.95 \times 10^{-8}$ m^3/mol. (B) Differences between the observed and calculated paramagnetic chemical shifts; the error bars are represented for the shift difference and are given by ($\Delta\delta_{pm}$ + 0.04 ppm) (see Material and Methods).

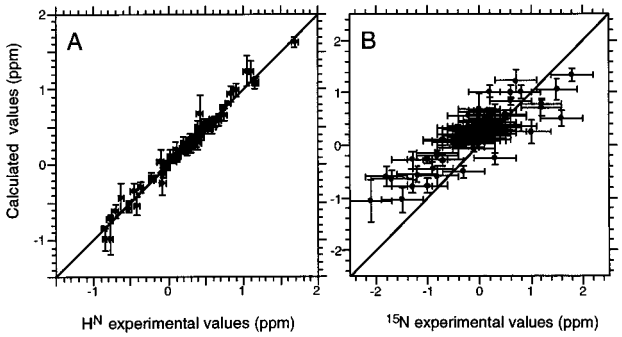

Figure 5. Comparison of the experimental paramagnetic chemical shifts of the *Rb capsulatus*. ferricytochrome *c′* H^N (A) and ^{15}N (B) with the shifts calculated with the results obtained from the H^{α} set. Values are $\alpha = 176°$, $\beta = 2°$, and $\Delta\chi_{ax} = -2.95 \times 10^{-8}$ m^3/mol. The H^N and ^{15}N chemical shifts of residues 69−74 correspond to the reassigned values (see text). The line corresponds to a perfect correlation, and error bars are represented for the measured shift (0.04 ppm for H^N and 0.4 ppm for ^{15}N) and the calculated shift ($\Delta\delta_{pm}$, see Material and Methods).

restricted ^{15}N set resulted in slightly different tilt angle and axial anisotropy. In the last stage, we have repeated the procedure with the combined sets of $^1H^{\alpha}$ and $^1H^N$ chemical shifts, and these final values are discussed. Uncertainties on the orientation and the principal component values have been estimated using Monte Carlo simulations[51] and are reported in Table 2. The *z* axis is perpendicular to the heme plane ($\beta < 2°$), and the axial component value is $\Delta\chi_{ax} = -2.94 \times 10^{-8}$ m^3/mol. We also performed the same calculations with the inclusion of the rhombic contribution in eq 2, which led to $\Delta\chi_{ax} = -2.95 \times 10^{-8}$ m^3/mol, $\Delta\chi_{rh} = 0.24 \times 10^{-8}$ m^3/mol, $\beta = 2°$, $\alpha + \gamma = 293°$, and $F/N = 3.33 \times 10^{-3}$ ppm^2 for the full combined set of $^1H^{\alpha}$ and $^1H^N$ protons (B subunit). The rhombic anisotropy is therefore very weak, and the introduction of the additional parameters $\Delta\chi_{rh}$ and γ does not significantly lower the global residual. Last, we have performed the calculations assuming the Cytc′ to be in a dimeric state as in the X-ray structure,[6] but no improvement of the fit was obtained.

Table 3. Chemical Shift of the Ligand Protons in *Rhodobacter capsulatus* Ferricytochrome *c′* and Related Compounds

	chemical shift (ppm)[a]					
proton[b]	caps[c]	palust[d]	gelat[e]	vinos[f]	molisch[f]	rubr[f]
methyl-18 (A)	85.1	81	82.5	82.0	81.0	83.4
methyl-2 (B)	76.7	76.5	79.5	72.7	80.4	77.0
methyl-12 (C)	73.3	68.6	69.5	70.2	68.2	67.5
methyl-7 (D)	62.7	61.6	65.0	62.7	62.5	63.4
propionate-13^1 (E)	47.6	43.4	57			
propionate-17^1 (F)	47.5	47.2	52			
propionate-17^1 (G)	44.6	45.7	34			
thiomethine-8 (H)	43.5	49.3	51			
propionate-13^1 (I)	35.2	42.1	30			
His122 β (β') (J)	31.1	37.4	29	28.7	32	36
His122 β' (β) (K)	29.1	36.6	28	25.7	31	32
thiomethine-3 (L)	18.1	20.9	17			
thiomethyl-3 (M)	10.5	10.0	11			
thiomethyl-8	7.1	5.8	8			
5-H		−11.9				−22
10-H		−16.4				−25
15-H		−21.8			−18	−30
20-H	−14[g]	−26.4			−25	−35

[a] Chemical shifts are referenced to the H_2O resonance. [b] Heme protons are named following the IUPAC recommendations. Letter in parentheses corresponds to the peak labeling in Figure 6. [c] This work, measured at 300 K, pH 6.0. [d] Ferricytochrome *c′* of *Rps. palustris* recorded at 313 K and pH 5.0.[12i] [e] Ferricytochrome *c′* of *Rc. gelatinosus* recorded at 295 K and pH 7.2.[12f] [f] Ferricytochrome *c′* of *C. vinosum*, *Rsp. molischianum*, and *Rsp. rubrum* recorded at 298 K and pH 5.[12d] Assignments are only tentative and are based on chemical shift values. [g] Assignment is only tentative (see text).

Assignment of the Iron(III) Ligand Protons. The spectrum of the ferriCytc′ of *Rb. capsulatus* is similar to those reported for other species: *C. vinosum*, *Rsp. rubrum*, *Rsp. molischianum*, *Rps. palustris*, and *Rc. gelatinosus*[12d−f,i] with four methyl resonances shifted downfield (Figure S1). Heme protons, which are broad resonances resolved from the diamagnetic envelope, have been assigned using a 2D NOESY experiment in ^2H_2O and are reported in Table 3 together with those of homologous cytochromes c′. First, the assignment was initiated at the four CH_3 signals at 85.1, 76.7, 73.3, and 62.7 ppm. They were assigned via chemical exchange correlations between the methyl resonances of the reduced form[39] and the oxidized form (data not shown). Using these assignments as starting points, we identified the propionate-13 and -17 α-protons as pairs of resonances giving strong NOE correlations to each other and from their correlations with Met-12 and Met-18, respectively. The correlations between the two 17 α-protons which are nearly overlapping were observed at a slightly lower pH, where they were better resolved. Met-3 and Met-8 have been assigned as giving the strongest correlations with Met-2 and Met-7, respectively. Moreover, these two resonances show NOE correlations with signals at 43.5 and 18.1 ppm that were further assigned to thiomethine-3 and thiomethine-8, respectively.

(50) The following nuclei were excluded from the fit. $^1H^{\alpha}$ set: 21, 23, 24, 27, 30, 31, 33−40, 43, 44, 56, 62, 63, 71, 73, 77, 97−100, 103, and 106 in subunit A; 23, 24, 27, 30−40, 44, 56, 62, 63, 71, 73, 77, 97−100, 103, and 106 in subunit B. $^1H^N$ set: 27, 39, 43, 60, 78, 93, 95, and 96 in subunit A; 27, 31, 39, 60, 78, 93, 95, 96 in subunit B. For $^1H^{\alpha} + {}^1H^N$ set: $^1H^{\alpha}$, 23, 24, 27, 30, 33−39, 43, 56, 59, 62, 63, 71, 77, 97−100, 103, 105, and 106; $^1H^N$, 8, 27, 31, 39, 43, 93, 95, 96, and 101 in subunit A; $^1H^{\alpha}$, 24, 27, 30, 31, 33−39, 56, 59, 62, 63, 69, 77, 97−100, 103, 105, 106, and 109; $^1H^N$, 27, 31, 39, 43, 60, 78, 95, 96, and 101 in subunit B.

(51) Cordier, F.; Caffrey, M.; Brutscher, B.; Cusanovich, M. A.; Marion, D.; Blackledge, M. *J. Mol. Biol.* **1998**, *281*, 341−361.

Table 4. Analysis of the Chemical Shifts for the Ligand Protons of *Rhodobacter capsulatus* Ferricytochrome *c*′

	chemical shift (ppm)[a]					chemical shift versus 1/*T*			
heme atom[b]	obs[c]	dia[c]	param[d]	dipolar[e]	contact[f]	slope[g]	interc[g]	slope′[h]	interc′[h]
methyl-18	85.1	3.60	81.5	6 ± 1	72.5	28.5	−10.0	24.8	−3.7
methyl-2	76.7	3.70	73	6 ± 1	67	27.4	−15.4	24.3	−10.1
methyl-12	73.3	3.74	69.6	6 ± 1	63.5	25.2	−10.9	22.2	−5.9
methyl-7	62.7	3.78	58.9	6 ± 1	53	19.4	−2.0	15.7	4.2
propionate-13[l]	47.6	i	44.1	7 ± 1	37	16.1	−6.3	13.4	−1.8
propionate-17[l]	47.5	i	44.0	7 ± 1	37	16.1	−6.3	13.4	−1.8
propionate-17[l]	44.6	i	41.1	5 ± 1	36	7.8	18	3.2[j]	25.8[j]
thiomethine-8	43.5	5.9	37.6	6 ± 1	31.5	15.8	−9.3	12.3	−3.5
propionate-13[l]	35.2	i	31.7	5 ± 1	26.5	8.8	6.1	6.1	10.7
His 122 β (β')	31.1	1.50[k]	29.6	−11 ± 4	40.5	4.8	15.2	8.0	15.3
His 122 β' (β)	29.1	1.50[k]	27.6	−11 ± 4	38.5	1.9[j]	24.4[j]	4.9	24.4
thiomethine-3	18.1	6.00	12.1	7 ± 1	5	6.6[j]	−4.2[j]	4.5[j]	−4.2[j]
thiomethyl-3	10.5	2.30	8.2	3 ± 1	5	0.1	7.4	0.2[j]	7.4[j]
thiomethyl-8	7.1	1.61	5.5	3 ± 1	2				
5-H		9.73		14 ± 4					
10-H		9.92		13 ± 4					
15-H		9.23		15 ± 4					
20-H	−14	9.99	−23	14 ± 4		−37			

[a] Chemical shifts are referenced to the H_2O resonance and are obtained at pH 6 and 300 K. [b] Nomenclature of the heme protons of the cytochrome *c*′ followed IUPAC recommendations. [c] Observed chemical shift in the oxidized state (obs) and in the diamagnetic CO complex (dia) are accurate to ±0.02 ppm. [d] Obtained from the difference obs − dia (see note *c*). [e] Calculated from the values of the magnetic susceptibility tensor determined in this work and the coordinates of the heme protons of the ferricytochrome *c*′ structure.[6] Uncertainties are estimated as described in Material and Methods. [f] Obtained from the difference param − dipolar (see notes *c*,*e*). [g] Slope (10^3 ppm K) and intercept value (ppm) at $T \rightarrow \infty$ in plot of the observed chemical shift versus 1/*T*. [h] Slope (10^3 ppm K) and intercept value (ppm) at $T \rightarrow \infty$ in plot of the observed chemical shift subtracted from the dipolar shift versus 1/*T*. The dipolar shift was calculated from the value at 300 K (dipolar) and was assumed to vary as $1/T^2$ with temperature. [i] Propionate signals have been observed at 3.5, 2.95, 2.87, and 2.75 ppm for the diamagnetic CO complex but have not been specifically assigned. A value of 3.5 ppm has been taken for each propionate α-proton. [j] Values for which a correlation coefficient lower than 0.99 were obtained in the least-squares fitting of the shift versus 1/*T* with a linear function. [k] Average value for the His122 β- and β'-protons.

Assignments are in agreement with those reported for *Rc. gelatinosus*[12f] and *Rps. palustris*[12i] ferriCytc′, as summarized in Table 3. By analogy with those assignments, the two remaining low-field signals at 31 and 29 ppm were further assigned to the β-protons of His122, and the very broad resonance (>1 kHz) observed around −14 ppm was tentatively assigned to a meso proton.[12d,i]

The ^{1}H chemical shifts and line widths of the heme ligand show large variations in the pH 5−10 range (Supporting Information, Figures S2 and S3). Most of the resonances shift upfield upon raising the pH (Supporting Information, Figure S1 and S2). Only the α-protons of the propionate-13 exhibit a different behavior, shifting downfield from 35 and 44 ppm at pH 5.1 to 49 and 59 ppm at pH 10.6. Two protons assigned to the β-protons of His122 broaden and become unobservable at pH 7.5. At high pH, we observed the appearance of very broad lines near 95 ppm which could be assigned to those protons by comparison with the behavior observed in other Cytc′.[12d−f,i] The broad resonance at −14 ppm, tentatively assigned to a meso proton, disappears at higher pH, whereas three new resonances appear near −14, −20, and −26 ppm at pH 9.5. Saturation of these resonances at pH 10.5 yielded no detectable NOEs with other protons, impeding their assignment. The pH-modulated transition which occurs in the pH 8−9 range has been linked to deprotonation of the axial imidazole ligand to imidazolate.[12b] Analysis of the methyl chemical shift variations indicates a pK_a of 8.91 ± 0.05 for this transition in *Rb. capsulatus*. During this transition, we observed a broadening of all the resonances exhibiting shift changes (e.g., the line widths of the heme methyl resonances go from ∼200 Hz at pH 6.0 to ∼300 Hz at pH 10.5 via a maximum near the pK_a, cf. Figure S2).

Contact Shift of the Ligand Protons. The magnetic susceptibility tensor has been derived from eq 2 using the experimental dipolar shifts for protons located more than 10 Å from the iron center, a situation for which the metal-centered hypothesis holds true. For closer protons, a rigorous calculation of the dipolar shift should include a ligand-centered contribution.[52] Nevertheless, this approach still provides an estimate for the dipolar shift which can be used, in turn, to derive the contact shift for the heme protons, the diamagnetic contribution being given by the assignment of the CO complex. The observed shifts of heme protons are split into their different contributions (Table 4). Positive contact shifts are found for the His122 β,β'-protons, the α-propionate protons, the pyrrolic methyl and thiomethine resonances, and the thiomethyl resonances, whereas a negative contact shift is obtained for the tentatively assigned meso proton.

The temperature dependence of the contact shift was investigated between 278 and 315 K by 1D NMR spectra. The observed chemical shifts apparently follow a Curie law (1/*T*). The intercepts at infinite temperature do not fall in the diamagnetic region (Table 4). Therefore, the dipolar contribution, previously estimated at 300 K, has been subtracted from the observed shifts, assuming that it would vary with $1/T^2$ as expected for $S = {}^5/_2$ hemoproteins (cf. eqs 3 and 4). The resulting shifts were plotted again versus 1/*T*, but intercepts were still out of the diamagnetic region, as illustrated in Figure 6 and Table 4.

Magnetic Susceptibility Measurements. The contribution of the $^3/_2$ spin state of *Rb. capsulatus* Cytc′ has been estimated to be about 40% by EPR.[10d,15b] Nevertheless, as pointed out previously,[53] this contribution could be modulated by adjusting the experimental conditions: the difference between the studied strains, the ionic strength, or the nature of the buffer salts. As we observed some primary sequence differences in our strain (see assignment section), we recorded the EPR spectrum at 4 K of a frozen solution of our Cytc′. The spectrum displays two principal signals centered at $g_1 = 5.73$ and $g_2 = 4.62$

(52) Bertini, I.; Luchinat, C. In *NMR of Paramagnetic Molecules in Biological Systems*; Lever, A. B. P., Gray, H. B., Eds.; The Benjamin/Cummings Publishing Co.: Menlo Park, NJ, 1986; pp 47−84.

(53) Imai, Y.; Imai, K.; Sato, R.; Horio, T. *J. Biochem. (Tokyo)* **1969**, *65*, 225−237.

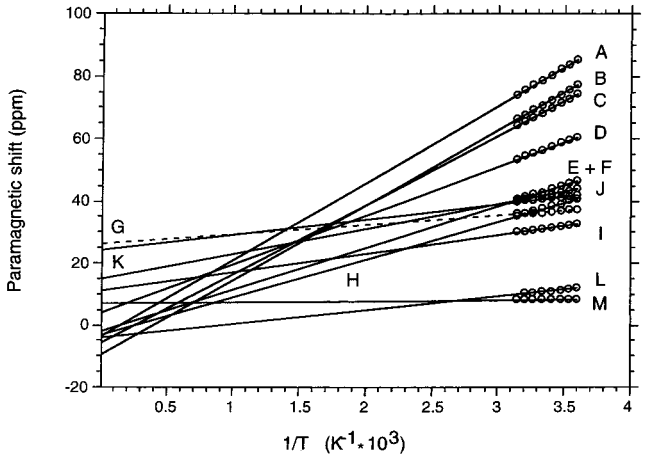

Figure 6. Curie plot of the contact shifts derived as the observed chemical shift corrected from the calculated dipolar contribution (see Table 4) for the heme protons of the *Rb. capsulatus* ferricytochrome *c′*. Labeling correspond to (A) Met-18, (B) Met-2, (C) Met-12, (D) Met-7, (E) Prop-13 α, (F) Prop-17 α, (G) Prop-17 α′, (H) thiomethine-8, (I) Prop-13 α′, (J) His122 *β*, (K) His122 *β*′, (L) thiomethine-3, (M) thiomethyl-3. The linearity of the contact shifts as a function of 1/*T* is in contrast with the pattern observed in quantum-admixed iron porphyrin models.

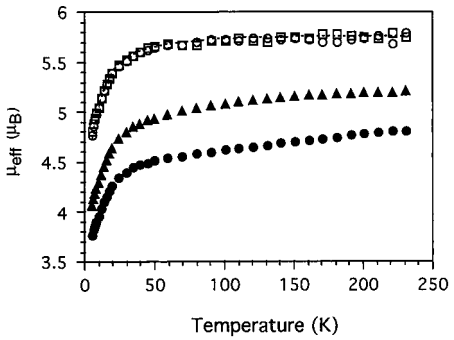

Figure 7. Temperature dependency of the molar effective magnetic moment of the *Rb. capsulatus* ferricytochrome *c′* for two values of the magnetic field. Open circle, 0.5 T; open square, 1 T. The dashed line through the data is the magnetic moment curve calculated using the model of Maltempo ($\Delta = -726$ cm^{-1} and $\lambda = 228$ cm^{-1}) corresponding to a (90% $^5/_2$, 10% $^3/_2$) quantum-admixed spin state. The full circle and full triangle correspond to the molar effective magnetic moment of either a (40% $^5/_2$, 60% $^3/_2$) or a (60% $^5/_2$, 40% $^3/_2$) quantum-admixed spin state, respectively. The molar effective magnetic moment in the range 5.6−5.7 μB is in good agreement with a predominantly $S = {}^5/_2$ spin state.

corresponding to a $g_{\perp\text{eff}} = 5.2$ (Supporting Information, Figure S4), which is identical to those values previously reported.[10d,15b] EPR results in the frozen state and NMR studies in solution then suggest different contributions of the $S = {}^3/_2$ state in the quantum admixed spin state for the Cytc′ of *Rb. capsulatus*. This could be due to spin state transitions occurring between 4 K and room temperature, which lead us to investigate the magnetic properties of Cytc′ of *Rb. capsulatus* as a function of the temperature. Figure 7 illustrates the temperature dependence of the molar effective magnetic moment observed in the ferriCytc′ sample for two applied magnetic fields. Surprisingly, no change of the shape of the experimental data indicative of a spin transition is observed over the range of temperatures studied. The molar effective magnetic moment above 100 K is between 5.7 and 6.0 μ_B (depending on the estimation of the number of moles in the sample) and thus is in good agreement with the value expected for 1 mol of isolated spin sextuplet:

Table 5. Calculated Zero-Field Splitting, Crystal-Field, and Spin−Orbit Coupling Constants for the Oxidized Form of the Cytochrome c′ of *Rb. capsulatus*

	$S = {}^5/_2$	quantum-admixed spin state	
parameters	spin state	free[a]	constrained[a]
N[b]	0.28	0.297	0.318
TIC 0.5[c]	3.7	−9.25	5.3
TIC 1[c]	5.13	−4.8	8.9
D (cm^{-1})[d]	12.3	14.3	
E (cm^{-1})	1.3		
Δ (cm^{-1})		−726	−30.4
λ (cm^{-1})		228	62
residual[e]	5.27	6.3	607

[a] In the constrained fit, the proportion of high- and intermediate-spin states was fixed to 40% $^3/_2$ and 60% $^5/_2$. [b] Number of micromoles of paramagnetic iron center in the sample. This value was fitted during the calculation. [c] Temperature-independent correction in 10^{-10} emu. [d] Calculated for the admixed spin state model from $D = \lambda^2/5\Delta$.[43] [e] Residual of the fit. Values were given in 10^{-15} emu^2·K^2.

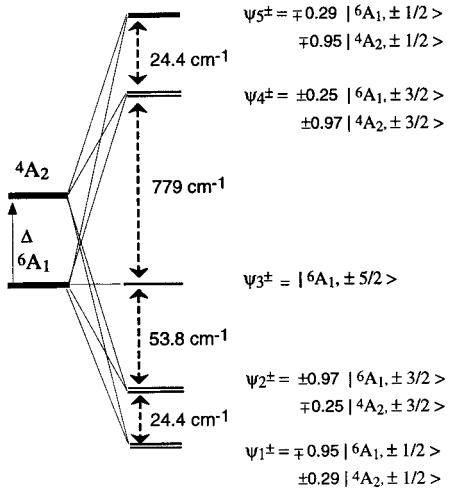

Figure 8. Energy levels for the heme-iron electronic state deduced from the magnetic susceptibility data using the model of Maltempo. Values are for the crystal field parameter $\Delta = -726$ cm^{-1} and the spin−orbit coupling constant $\lambda = 228$ cm^{-1}. Arrows correspond to the energy separation between the different sublevels. The respective contributions of the pure spin state wave functions in the mixed doublets are given.

5.95 μ_B. None of the excited states with a spin value different from the ground state is thermally accessible, at least below 1000 K, as indicated by the absence of a wide variation in the effective magnetic moment between 100 and 250 K. The difference observed between the isofield curves at 0.5 and 1 T indicates the presence of a large ZFS interaction[42] (Supporting Information, Figure S5).

The data have been fit using two models (see Table 5). The first one assumes a pure $S = {}^5/_2$ spin state, while the second considers two neighboring spin states, $^5/_2$ and $^3/_2$, quantically mixed through spin−orbit interactions as developed by Maltempo.[14] Using the simplest model of an isolated pure spin state gives very good agreement between the experimental data and the calculation. We also found a D value (12.3 cm^{-1}) and a low rhombicity ($E = 1.3$ cm^{-1}) in the range of those observed in high-spin compounds.[54] The solid lines shown in Figures 7 and S5 correspond to the adjustment resulting from the Maltempo model. In Figure 8, the scheme of the energy levels deduced from the adjustment and the respective contribution of the $^5/_2$ and $^3/_2$ spin state in the different sublevels are given.

(54) Palmer, G. In *The Porphyrins*; Dolphin, D., Ed.; Academic Press: New York, 1979; Vol. 4, pp 313−353.

Basically, the spin state of the iron in the Cytc′ can be described as essentially a $^5/_2$ state. The contribution of the $^3/_2$ state is indeed weak, less than 10% in the lower Kramer doublet. The separation in energy between the $^6A_1$ and $^4A_2$ states or crystal-field parameter Δ is -720 cm^{-1}, and the spin−orbit coupling constant λ is 228 cm^{-1}. These values correspond to a D value of 14.5 cm^{-1} as inferred from the expression of D.[43] However, a slight disagreement between the data and the fit can be observed at very low temperatures for the magnetic field value of 1 T. Last, we fit the data keeping the spin state proportions constant (i.e., the Δ/λ ratio) corresponding to those deduced from EPR measurements and leaving free the other parameters. The results are reported in Table 5 but do not give a better fit of the experimental data, as indicated by the higher value of the residual.

Discussion

In this study, we have characterized the oxidized paramagnetic form of the cytochrome *c′* of *Rb capsulatus*. For the first time, the amplitude and orientation of the magnetic susceptibility tensor in a ferriCytc′ have been determined as well as the contribution of the Fermi shift to the heme proton chemical shifts. This allows us to gain some insight into the magnetic properties of this protein.

Assignment of the Diamagnetic Form. The present assignment achieved on the *Rb. capsulatus* Cytc′ CO complex represents the most complete assignment of a cytochrome *c′*, which was allowed by ^{15}N labeling and the absence of paramagnetism. Thus, the secondary structure has been unambiguously determined for the whole polypeptide chain, including the C-terminal region missing in the paramagnetic forms.[12,39] The location of the secondary structure in the CO complex does not show significant differences from those observed either for the paramagnetic forms in solution[12,39] or in the crystallographic structures.[6,8] In addition, we anticipate that the increased number of assigned residues (i.e., 14−18 and 118−129) and observable NOEs between the heme and protein moieties will facilitate the structure calculation for *Rb. capsulatus*, especially in the heme vicinity.

Structural Properties in Solution of the Oxidized Form. Structural determinants of the unusual EPR properties of the cytochromes *c′* remain to be understood. As yet, 3D structures of ferriCytc′ have only been obtained in the solid state by X-ray crystallography, which led us to address the question of the solution structure of these proteins. Dipolar shifts inferred from the assignment of the oxidized and the diamagnetic forms have allowed us to probe for structural changes either between the five-coordinate ferric state and the CO complex ferrous state or between the solution structure and the crystal structure. Generally, protons that exhibit chemical shifts in poor agreement with the calculated dipolar shifts are interpreted as undergoing such changes.[41] The very good agreement obtained for the $^1H^\alpha$ shifts suggests that no large-scale structural change in the backbone is observed between these two redox forms or between the oxidized form in solution or in the crystalline state. Outliers (according to the criterion defined in the Materials and Methods section) are primarily located in loop regions. The fair agreement of the $^1H^N$ shifts suggest that no major change in the hydrogen bond network takes place between the different redox forms. For backbone ^{15}N, the agreement is definitely worse than for ^{1}H, as previously reported for the cytochrome b_5[55], for the reduced form of the Cytc′,[39] and for cytochrome *c*.[56] In this last case, subtle variations of the NH bond in the heme vicinity have been invoked to explain the different behavior.[56] These results, therefore, indicate that no large change takes place in solution for the ferriCytc′ with respect to the solid-state structure.[6]

Redox-dependent structural changes could be expected in the heme vicinity because of the addition of the CO ligand and the displacement of the iron into the heme plane induced by the hexacoordination. Unfortunately, nuclei in the heme cavity were difficult to assign in the oxidized state because of their short paramagnetic relaxation times. Moreover, given the large uncertainty on the calculated dipolar shift in the heme vicinity, the deviations observed between experimental and calculated values are not large enough to be interpreted in terms of structural changes. In contrast, analysis of the heme contact shifts allows us to test the orientations of the heme side chains in the two redox forms. The contact shift for the propionate α-methylenes is indeed given by

$$\delta_{con} = A \cos^2 \xi$$

where A accounts for the spin density on the adjacent α-carbon and ξ is the dihedral angle of the $C^\pi-C^\alpha-H^\alpha$ plane with the C^π z axis. Therefore, as shown in previous studies,[57] the ratio of the contact shifts for a pair of protons can provide detailed information on the orientation of the propionate groups:

$$Z_i = \delta_{con,i}(\alpha)/\delta_{con,i}(\alpha') = \cos^2 \xi_i/\cos^2 \xi'_i$$

with $\xi_i + \xi'_i = 120°$ (i = 13 or 17).

The orientation of the propionate-17 group is nearly symmetric in view of the small difference in chemical shifts of the propionate-17 α- and α′-protons ($Z_{17ox} \approx 0.96$). In contrast, the propionate-13 α-proton, which is closer to Met-12, exhibits a smaller contact shift than the α′, and the ratio $Z_{13ox} \approx 0.73$ would correspond to $\xi_{13} \approx 63°$ and $\xi'_{13} \approx 57°$, so the $C^\alpha-C^\beta$ bond is tilted toward the direction opposite to Met-12. In the oxidized form, the crystallographic structure[6] shows that both propionate groups have a similar global orientation, with the $C^\alpha-C^\beta$ bond in the opposite direction to the Fe−His vector (this can be compared to the results for the reduced form as discussed below). In the reduced form,[39] resonances for the propionate-17 group are very different: the α-proton nearest Met-18 has a larger contact shift, and $Z_{17rd} \approx 2.1$ indicates that $\xi_{17} \approx 54°$ and $\xi'_{17} \approx 66°$. Thus, the methylene-17 group is rotated counterclockwise by 6° in the reduced form. In the reduced form, the propionate-13 α-proton exhibits the largest contact shift ($Z_{13rd} \approx 1.4$) and $\xi_{13} \approx 57°$ and $\xi'_{13} \approx 63°$. Thus, the methylene-13 group is rotated clockwise by 6°. The propionate-13 or propionate-17 α-protons (as opposed to α′), which correspond to the geminal proton closest to Met-12 or Met-18, respectively, in the oxidized state, were identified in the reduced form via exchange peaks observed between the two forms (data not shown). These resonances in the reduced form appear to give NOE correlation with Met-12 (or Met-18), which indicates that the global orientation of the propionate groups is not inverted upon reduction. In contrast, in the butylisocyanide-ferroCytc′ complex, the orientation of the propionate-17 group

(55) Guiles, R. D.; Basus, V. J.; Sarma, S.; Malpure, S.; Fox, K. M.; Kuntz, I. D.; Waskell, L. *Biochemistry* **1993**, *32*, 8329−8340.

(56) Boyd, J.; Dobson, C. M.; Morar, A. S.; Williams, R. J. P.; Pielak, G. J. *J. Am. Chem. Soc.* **1999**, *121*, 9247−9248.

(57) Pande, U.; La Mar, G. N.; Lecomte, J. T. J.; Ascoli, F.; Brunori, M.; Smith, K. M.; Pandey, R. K.; Parish, D. W.; Thanabal, V. *Biochemistry* **1986**, *25*, 5638−5646. Thanabal, V.; La Mar, G. N.; de Ropp, J. S. *Biochemistry* **1988**, *27*, 5400−5407.

has been found to be inverted, with the $C^{\alpha}-C^{\beta}$ bond tilted toward the Fe−His direction, due to rearrangement of the H-bonding pattern, as observed by X-ray crystallography.[6] Our data indicate only a slight reorientation (∼6°) of both propionate groups between the oxidized and the reduced forms. Moreover, Met-2 and Met-7 exhibit NOE connectivities with thiomethyl-3 and thiomethyl-8, respectively, but not with thiomethine-3 and thiomethine-8, which suggests that the thiomethine-3 and thiomethine-8 are oriented toward their respective meso protons. This geometry for the thioether linkages is therefore consistent with the X-ray structure[6] and is similar to homologous cytochromes *c′*.[12e,f,i]

Contact Shift Analysis. Values of the ligand contact shifts in the oxidized form were determined from the assignment of the diamagnetic form and the dipolar shifts calculated from the magnetic tensor. For His122, we found a very large positive contribution of the contact on the C^{β}, about +40 ppm. This is in agreement with the large contact shift expected from the interaction of the monopopulated d_{z^2} orbital with the ligand. For the heme protons, the contact shift was found to be the major contribution to the paramagnetic shifts. According to model compounds, high-spin five-coordinate Fe(III) is characterized by large downfield pyrrole shifts (∼80 ppm) and by upfield meso shifts (∼−50 ppm), with the former due to a large σ-delocalization of the half-occupied $d_{x^2-y^2}$ orbital and the latter arising from π-delocalization from the d_{xz} and d_{yz} orbitals to the porphyrin vacant orbital 4e(π^*), presenting large wave function coefficients at the meso positions.[21] In the $S = {}^3/_2$ state, where the $d_{x^2-y^2}$ orbital is unoccupied, no σ-delocalization at pyrrole positions takes place, and a dominant porphyrin → metal π-delocalization from the orbital 3e(π) has been invoked to explain the large downfield shift observed for pyrrolic positions in iron porphyrin complexes.[21,58] In *Rb. capsulatus* Cytc′, the large positive contact shifts observed at the methyl pyrrolic positions (from 50 to 72 ppm) and the observation of contact shifts of the same sign and decreasing amplitude on the thioether links 4 and 8 are clearly in agreement with spin density originating from σ-delocalization and from a half-occupied $d_{x^2-y^2}$ orbital, similar to that of $S = {}^5/_2$ heme proteins. Moreover, the heme resonances globally obey Curie's law, which suggests that, in the range of temperature considered, no variation of population takes place between different spin states. This behavior is different from those of spin-admixed ($S = {}^3/_2, {}^5/_2$) model compounds in which large anti-Curie variations of the pyrrolic protons are observed, constituting a hallmark for these compounds.[21] From this point of view, it would be surprising if *Rb. capsulatus* ferriCytc′ does not exhibit this feature if the contribution of $S = {}^3/_2$ is equal, as inferred from EPR results at low temperature, to 40% in the quantum-admixed spin state. The pH dependency of the proton resonances in *Rb. capsulatus* appears to be very similar to those of the *Rsp. molischianum*, *Rps. palustris*, and *Rsp. rubrum* species, in particular for the protons of propionate-13. This is in contrast to the case with *C. vinosum*, in which the chemical shifts of these protons move downfield below the pK_a and upfield above the pK_a. In the same way, the broadening of the heme resonances shows only an increase upon raising the pH in *C. vinosum*, whereas in the four other species the broadening exhibits a maximum near the pK_a. In the cytochromes *c′*, the positions of the meso protons have been proposed as an indicator of the intermediate-spin character of the complex, with a farther upfield shift corresponding to a lower $S = {}^3/_2$ contribution.[12d] In *C. vinosum*, reported as presenting significant mixed spin states, the meso proton resonances are observed only at alkaline pH and disappear at neutral or acidic pH, presumably shifted downfield and therefore hidden under the diamagnetic envelope. The *Rb. capsulatus* ferriCytc′ exhibits a signal at pH 6 tentatively assigned to meso proton(s). At pH 10, this signal disappears, and the spectrum exhibits three broad signals around −20 to −35 ppm, similar to those observed at acidic pH for the meso protons in high-spin species (−10 to −40 ppm).[12d] In *Rb. capsulatus*, the influence of pH on the upfield resonances appears, then, to be closer to those in *C. vinosum* than in high-spin species and, accordingly, could be interpreted as arising from a significant contribution of $S = {}^3/_2$ at room temperature. On the other hand, at neutral pH, the contact shift on this meso position could be estimated to be about −40 ppm, in agreement with a large metal → porphyrin π-delocalization as described for high-spin Fe(III).

Magnetic Properties. At room temperature, the magnetic susceptibility tensor in *Rb. capsulatus* ferriCytc′ was found to be essentially axially symmetric, with its principal axis direction along the normal to the heme. A similar orientation in the molecular frame has been found for the high-spin iron(III) metaquomyoglobin.[24] No orientation of the susceptibility tensor in a pure $S = {}^3/_2$ hemoprotein is known, and it is therefore not possible to directly compare our results. However, in the two other *S* states, where the d electron sphere is not symmetrical, significant deviations of the *z* axis of the susceptibility tensor are observed: from 10° to 20° in the $S = {}^1/_2$ state[59] and from 30° to 50° in the $S = 2$ state.[39,60] So, some similar deviations from the heme normal could be expected for an asymmetrical state such as $S = {}^3/_2$. In contrast, the $S = {}^5/_2$ state presents only a very weak deviation from this direction.[24] Contact shift analysis strongly suggests that, at room temperature, the $d_{x^2-y^2}$ orbital is half-occupied. If one assumes that the spin value is ${}^5/_2$ at room temperature, the *D* value derived from $\Delta\chi_{ax}$ (−2.94 10^{-8} m^3/mol) in eq 3 is +10.4 cm^{-1}, which is very similar to the values of +9.7 cm^{-1} determined using NMR in metaquomyoglobin,[24] or +12 cm^{-1} as proposed in *Rps. palustris* ferriCytc′.[12i] The rhombicity is low, the ZFS rhombic parameter *E* being 0.3 cm^{-1}. Similar *D* values (+5 to +15 cm^{-1}) as well as generally very weak rhombicity have been determined in high-spin ferric compounds by EPR, magnetic susceptibility measurements, or Mössbauer spectroscopy.[54,61] Magnetic susceptibility measurements are in agreement with the NMR results at room temperature. In particular, the first-order variation of the molar effective magnetic moment as a function of the temperature is very similar to those observed in weakly spin-mixed (${}^5/_2$, ${}^3/_2$) (triflato)aquoiron(III) porphyrin complex.[62] We do not observe any change in the shape of the experimental data indicative of a spin transition over the range of temperature. In contrast, a striking feature of the highly spin-mixed (${}^5/_2$, ${}^3/_2$) states is their temperature behavior, presenting different slopes due to the successive populations of the energy levels.[20,63] From this point of view, using a (60% ${}^5/_2$, 40% ${}^3/_2$) quantum-admixed

(58) Boersma, A. D.; Goff, H. M. *Inorg. Chem.* **1982**, *21*, 581−586.

(59) Shokhirev, N. V.; Walker, F. A. *J. Am. Chem. Soc.* **1998**, *120*, 981−990 and references therein.

(60) Bougault, C. M.; Dou, Y.; Ikeda-Saito, M.; Langry, K. C.; Smith, K. M.; La Mar, G. N. *J. Am. Chem. Soc.* **1998**, *120*, 2113−2123.

(61) Münck, E. In *The Porphyrins*; Dolphin, D., Ed.; Academic Press: New York, 1979; Vol. 4, pp 379−423.

(62) Gismelseed, A.; Bominaar, E. L.; Bill, E.; Trautwein, A. X.; Winkler, H.; Nasri, H.; Doppelt, P.; Mandon, D.; Fischer, J.; Weiss, R. *Inorg. Chem.* **1990**, *29*, 2741−2749.

(63) Mitra, S.; Marathe, V. R.; Birdy, R. *Chem. Phys. Lett.* **1983**, *96*, 103−107. Gupta, G. P.; Lang, G.; Reed, C. A.; Shelly, K.; Scheidt, W. R. *J. Chem. Phys.* **1987**, *86*, 5288−5293. Gupta, G. P.; Lang, G.; Young, J. L.; Scheidt, W. R.; Shelly, K.; Reed, C. A. *Inorg. Chem.* **1987**, *26*, 3022−3030. Scheidt, W. R.; Osvath, S. R.; Young, J. L.; Reed, C. A.; Shaevitz, B.; Gupta, G. P. *Inorg. Chem.* **1989**, *28*, 1591−1595.

spin model leads to a very poor fit of the experimental data with very low values of the spin−orbit coupling constant (see Table 5). Furthermore, when we considered the Maltempo model leaving the contribution of the $^3/_2$ state as a variable parameter, we found only a weak contribution of the $^3/_2$ state in the spin state (about 10%), and the derived D value is 14 cm^{-1}. No rhombicity was introduced in this model for the fitting procedure, but assuming the $^5/_2$ spin state as an approximation of the spin state leads us to derive a ZFS axial parameter D of 12.5 cm^{-1} and a ZFS rhombic parameter E of 1.6 cm^{-1}, indicating only a weak deviation from the axial symmetry. In the same way, estimation of the rhombicity from the two components of the $g_\perp$ signal gives an E value of 0.6 cm^{-1}. Fitting of the susceptibility data leads to a spin−orbit coupling constant of 228 cm^{-1} and a crystal field parameter of −726 cm^{-1}. The spin−orbit value is lower than those expected for high-spin ferric ion, ∼400 cm^{-1},[64] but is in the 150−300 cm^{-1} range determined in ferric hemoproteins or model complexes.[62,63]

In summary, the ferriCytc′ of *Rb. capsulatus* exhibits magnetic properties whose characters are primarily those of high-spin compounds, i.e., an axial magnetic susceptibility tensor and an axial susceptibility anisotropy compatible with those predicted from the classical high-spin D value (around 10 cm^{-1}). The contact shifts on the pyrrolic positions are indicative of large σ-delocalization and a half-occupancy of the highest d orbital of the iron, and the heme resonance behavior is similar to other high-spin cytochromes *c*′. Moreover, treatment of the susceptibility data using the model of Maltempo indicates only a weak contribution of the $S = {}^3/_2$ spin state. However, these results are not in agreement with the rather high contribution of the $S = {}^3/_2$ spin state in *Rb. capsulatus* which can be deduced from EPR measurements at 4 K using the same model, and it is still difficult to explain this discrepancy. It must be noted that this situation is also observed for *Rps. palustris*, for which EPR results predict a high $S = {}^3/_2$ contribution, whereas a pure high-spin state prevail from NMR results.[12d] Supplementary NMR and susceptibility studies of ferriCytc′ presenting a high $S = {}^3/_2$ contribution are clearly needed to explain this point.

(64) Abragam, A.; Bleaney, B. In *Electron Paramagnetic Resonance of Transition Ions*; Dover Publications Inc.: New York, 1986.

Acknowledgment. We thank Dr. Michel Jaquinod for electrospray mass spectrometry experiments, and Dr. Jean-Marie Mouesca and Dr. Catherine Bougault for helpful discussions. This work has been supported by the Centre National de la Recherche Scientifique, the Commissariat à l'Energie Atomique, Molecular Simulations Inc., and NIH grant GM21277. This is publication no. 722 of the Institut de Biologie Structurale "Jean Pierre Ebel". P.T. was a recipient of a CEA Ph.D. fellowship.

Supporting Information Available: Five tables containing the temperature dependence of the sample holder magnetic susceptibility for an applied field strength of 0.5 T, the magnetic susceptibility data of the protein sample recorded for applied field strengths of 0.5 and 1 T, the assignments for the ^{1}H and ^{15}N chemical shifts of *Rb. capsulatus* ferrocytochrome *c*′ carbon monoxide complex, and the reassignments for the ^{1}H, ^{13}C, and ^{15}N chemical shifts of *Rb. capsulatus* ferricytochrome *c*″; five figures presenting the 1D spectra, the chemical shifts of the heme protons resonances, and the line width of methyl-18 as a function of pH, the EPR spectrum at 4.2K of the *Rb. capsulatus* ferriCytc′ and the molar magnetization versus $\beta H/kT$ (PDF). This material is available free of charge via the Internet at http://pubs.acs.org.

JA0011663